## ARTICLE

# Single-atom nickel confined nanotube superstructure as support for catalytic wet air oxidation of acetic acid

Chengyu Jin[1,2,4], Lei Ma[3,4], Wenjing Sun [1], Peiwei Han[3], Xiangdong Tan[1,2], Huiling Wu[1,2], Mengyang Liu[1,2], Haibo Jin[3], Zhongshuai Wu[1], Huangzhao Wei[1]* & Chenglin Sun[1]*

Single-atom confined materials (SACMs) have been widely researched as catalysts in many fields within recent years. However, this class of materials may not only serve as a catalyst but also as a support material for certain reactions. Here we propose a general strategy to use SACMs as supports for tuning loaded noble metal (e.g., Ru) nanoparticles with enhanced catalytic activity. As a proof of concept, a nickel single-atom confined nitrogen-doped carbon nanotube (NCNT) superstructure is prepared as a support to load noble metal Ru for catalytic wet air oxidation of acetic acid. Improved catalytic activity with a mineralization rate of ~97.5% is achieved. Further, adsorption configurations based on DFT calculations also confirm our deduction that the introduction of single-atom Ni changes the intrinsic property of NCNTs and affects the loaded active Ru nanoparticles.

[1] Dalian Institute of Chemical Physics, Chinese Academy of Sciences, Dalian 116023, China. [2] University of Chinese Academy of Sciences, Beijing 100049, China. [3] Beijing Key Laboratory of Fuels Cleaning and Advanced Catalytic Emission Reduction Technology/College of Chemical Engineering, Beijing Institute of Petrochemical Technology, Beijing 102617, China. [4] These authors contributed equally: Chengyu Jin, Lei Ma. *email: whzhdicpwtg@dicp.ac.cn; clsun@dicp.ac.cn

Single-atom catalysts (SACs) have attracted lots of attentions for maximizing atom-utilization efficiency in recent years and the systematic progress on preparation strategies of SACs have achieved, which provide solid foundation for SACs in various applications[1,2]. The SACs often receive high catalytic activity due to the ultrahigh atom dispersion and unique con-figuration[1], while the anchored single atom may also affect the intrinsic property of base material and provide an new oppor-tunity for its application, especially, the SACMs. For many noble metals, the catalytic performance is strongly related to the char-acters of the supporting materials and the interaction between active site and supporting material is very important for the catalyst design[3]. Thus, exploring the new application of the single-atom dispersed material will be very meaningful.

Carbon nanotubes (CNT) possess high charge-transfer ability, by which the curved graphene sheets are composed of sp2 hybridized carbon. Doping N atom into CNT (NCNT) will alter the property of CNT and this strategy will also provide the coordinate sites for metal atom anchoring into carbon frame-work[4]. Zhao et al. adopted solid-state diffusion method producing single Ni atoms coordinated in NCNTs, which exhibited superb catalytic $CO_2$ reduction reaction performance[5]. Fu and co-workers reported that the transition metals (Fe, Co, Ni, Cu et al.) can be used as promoters to enhance catalytic performances of noble metal catalysts for the reactions involving oxygen activa-tion[6].These progresses inspired us to design a single-atom Ni confined NCNTs (Ni-NCNTs) as a new modified support to tune the activity of the loaded Ru nanoparticles (NPs). However, the traditional in-situ synthesis of Ni-NCNT is difficult to control the size of nanotube and achieve mass production. Thus, we here adopt the in-situ synthesis method to construct Ni-NCNTs superstructure on activated carbon (Ni-NCNT/AC), which is expected to dramatically improve the utilization of Ni-NCNTs and elevate the special surface area (SSA) of the Ni-NCNTs support at a proper level with an internal base material. Acetic acid is one of the most refractory organics for catalytic wet air oxidation (CWAO), which was regarded as the route dead-end of the phenol oxidation schedule proposed by Devlin and Harris[7]. Ru catalysts with zero-valence Ru ($Ru^0$) was proposed to be the best catalyst for acetic acid degradation[8]. However, the perfor-mance of catalysts with $Ru^0$ is not very desirable due to the interaction between $Ru^0$ and the support which $Ru^0$ NPs will transfer electrons to support (e.g., metal oxide) and decrease the electron density of the metal centers for activating the reactants or the partial oxidation during CWAO process[9].

Here we present a Ni single-atom confined NCNT super-structure Ni-NCNT/AC, in which the Ni single atoms were confined into the NCNT at a relatively high atomic rate (0.35–0.88%) through coordination of doped nitrogen. Then, Ru NPs are loaded on the acid cleaned surface after thermal reduc-tion, and this resulting catalyst was applied for the CWAO of acetic acid. Remarkably, Ru NPs supported on the single-atom doped NCNT superstructure (named as Ru@Ni-NCNT/AC) possesses extremely high activity for CWAO of acetic acid. The mineralization rate of acetic acid using Ru@Ni-NCNT/AC is as high as 97.5%, which is much higher than that of traditional Ru catalyst supported on $TiO_2$ and activated carbon (AC)[7,10]. Based on the characterization of catalysts, we propose the introduction of Ni promotes the catalytic activity of active metal Ru through an electron donor effect. The results of DFT calculation also prove the promoting effect of Ni's introduction.

## Results

### Preparation and morphological features of Ni-NCNT/AC. We firstly fabricated the Ni-NCNTs on the surface of the acated

carbon to obtain Ni-NCNT/AC support which possesses similar specific surface area with AC support. Massive Ni-NCNTs with relatively uniformed tube size cover the surface of the active carbon material (Fig. 1a). After acid cleaning process to remove Ni and NiO on the surface and partially in the tube of the pristine Ni-NCNT/AC, Ru was loaded on the surface by impregnation method with a following calcination. The Ru NPs on the surface of Ni-NCNT/AC are not much uniform and some of them are much larger than the NPs on AC surface (Fig. 1b and Supple-mentary Fig. 1) which is possibly caused by the hydrophilic property of NCNTs surface and relatively low specific surface area, resulting in poor dispersion of the Ru precursor (Supple-mentary Fig. 2 and Supplementary Table 1). However, the unexpectedly improved catalytic activity with larger particle size has gained our interest for exploring the structural specificity of Ru@Ni-NCNT/AC.

Here we observed that there are massive nanotubes covered the surface of AC constructing Ni-NCNT/AC superstructure (Fig. 1a) and Ru NPs and few clusters were supported on the surface of Ni-NCNT/AC (Fig. 1b and Supplementary Fig. 7). High-angle annular dark field scanning transmission electron microscopy (HAADF-STEM) shows that Ni single atoms are dispersed well in NCNT, in which the light spots correspond to the single-atom Ni anchored in the curved graphene sheet of NCNT (Fig. 1c, d). From the EDS mapping (Fig. 1e, f), we also can gain that the dispersion of the element Ni match well with that of the element N on the NCNT and the content of single-atom Ni ranges 0.35–0.88 at% (Supplementary Fig. 3). High-resolution XPS spectra of Ru@Ni-NCNT/AC show that the N 1s peak can be deconvoluted into four different peaks at ~398.6, ~399.4, ~400.9, and ~404.8 eV, attributing to pyridinic N (47.93%), pyrrolic N (27.96%), graphitic N (18.93%), and oxidized N (5.18%), respectively (Supplementary Fig 4 and Supplementary Table 2). The relatively high percentage of pyridinic N (47.93%) could indicate the high loading of Ni single atoms since the pyridinic N is generally believed to be served as the coordinating sites for transition metal species[11].

### X-ray absorption spectroscopy of Ni-NCNT/AC. The X-ray absorption fine structure (XAFS) was performed to confirm the possible bonding between Ni and the light elements. As shown in the normalized Ni K-edge X-ray absorption near edge structure (XANES) spectra (Fig. 2a), the position of the rising edge for Ni-NCNT/AC is located between those for Ni foil and the NiO, indicating that the average oxidation state of Ni in Ni-NCNT/AC is between $Ni^0$ and $Ni^{2+}$. The $k_3$-weighted Fourier transform spectra of the Ni K-edge extended X-ray absorption fine structure (EXAFS) demonstrates that peak at 1.46 Å, corresponding to Ni–N first shell, is clearly observed in Ni-NCNT/AC[12], and no obvious Ni–O bond is observed, compared with the K-edge EXAFS spectra of NiO, indicating that the surface of Ni-NCNT/ AC were well cleaned and no Ni NPs appeared on the surface of Ni–NCNT/AC. The Ni-Ni bonds observed in EXAFS spectra of Ni–NCNT/AC ascribed to the Ni NPs inside the nanotube (Fig. 2b). The wavelet transforming (WT) plot of Ni–NCNT/AC also display the different images from Ni foil, NiO. The intensity maximum at 6.5 Å$^{-1}$ in Ni-NCNT/AC should ascribe to Ni-N, which differ from 7.2 Å$^{-1}$ in NiO and 8.5 Å$^{-1}$ in Ni foil (Fig. 2c–e). These results further confirmed that the metal Ni was atomically dispersed in the wall of the NCNTs at a relatively high ratio, and there must be some interaction between Ru NPs and Ni–NCNT/AC resulting in the improved catalytic activity. Thus, we proposed an assumption that the graphene structure of the NCNTs possesses high electron-transferring property so that the anchored Ni atom may diffuse their outer electron on the
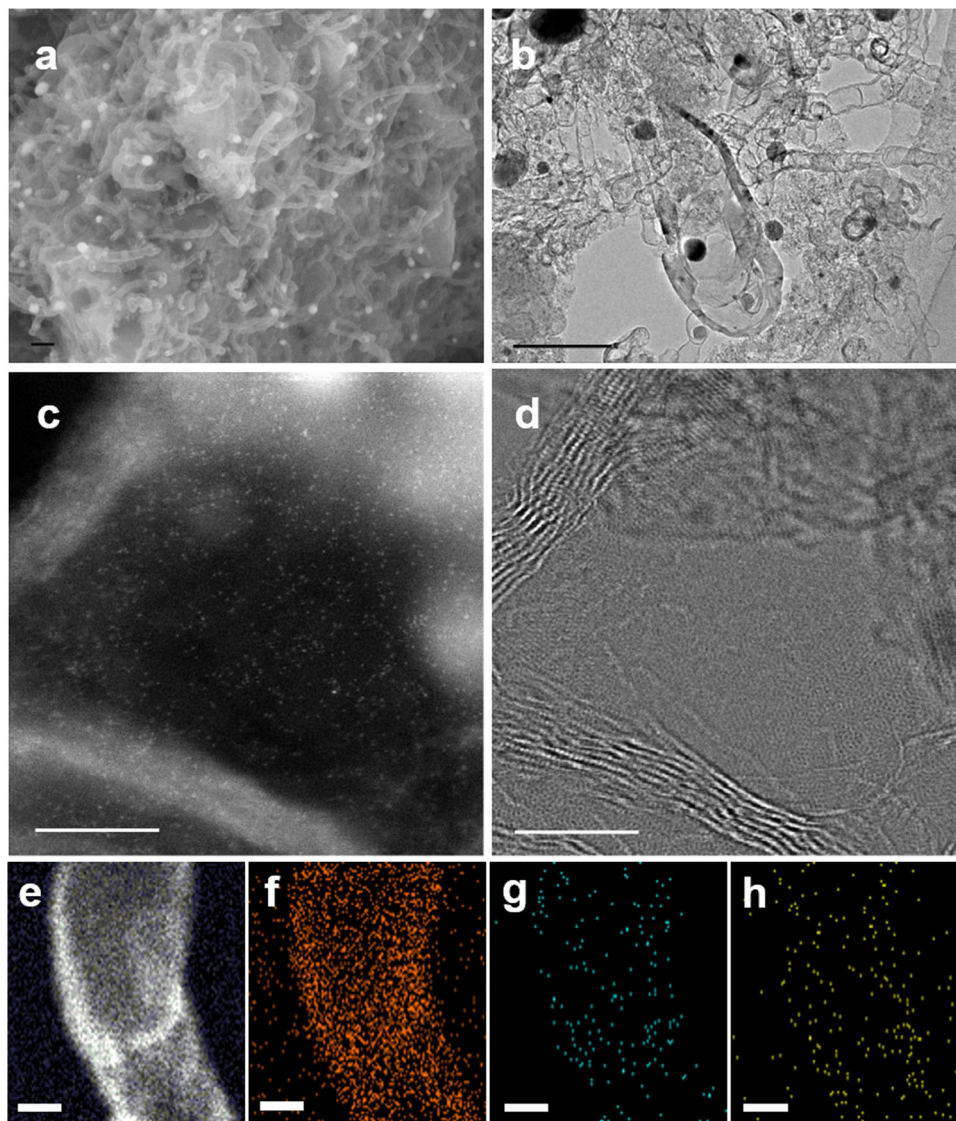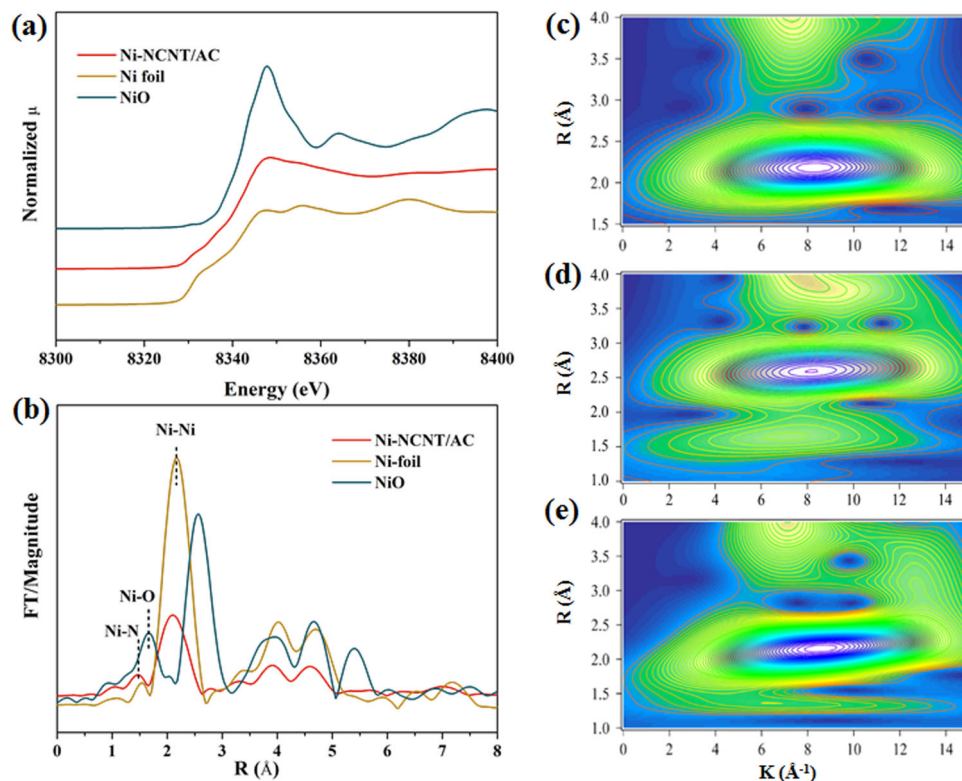
**Fig. 1** Structural characterization of the Ni-NCNT/AC and Ru@Ni-NCNT/AC. **a** SEM image of the pristine Ni-NCNT/AC. **b** TEM image of Ru@Ni-NCNT/AC. **c**, **d** HAADF-STEM images of shell of nanotube on Ni-N-CNT/AC; **e** EDS mapping of Ni-NCNT/AC. **a**, **b** scale bar 100 nm. **c**, **d** scale bar 5 nm. **e**–**h** scale bar 10 nm.

neighboring atoms and affect the electronegativity of the NCNT. This action will efficiently modify the NCNT support and make this material metal-like property to promote the main catalytic site.

**Catalyst evaluation in the CWAO system**. The catalysts were evaluated in the CWAO system with total organic carbon (TOC) removal of acetic acid solution as evaluation index (Fig. 3). Without catalyst, the TOC removal in WAO system was just 6.7% after the reaction. the conventional catalysts like Ru@TiO₂ and Ru@AC in CWAO system can promote the degradation of acetic acid in the CWAO system. But the TOC removal using Ru@TiO₂ (32.3%) and Ru@AC (65.3%) is not very desirable. Surprisingly, the CWAO system with Ru@Ni-NCNT/AC almost mineralized the acetic acid completely (TOC removal: 97.5%), while the Ni-NCNT/AC with or without acid-cleaning show low catalytic activity towards degradation of acetic acid (TOC removal: 16.3% and 12.8%) (Fig.3 and Supplementary Fig. 8). That means the main active sites of catalyst for CWAO of acetic acid is Ru NPs and Ni–NCNT/AC could be an excellent support to promote the Ru NPs. We also prepared Ru@NCNT/AC and

Ru@NCNT catalysts (Fig. 3 and Supplementary Fig. 9) as comparison to observe the influence of single-atom Ni, while the Ru@NCNT/AC just achieved TOC removal of 52%. This result is even lower than that of Ru@AC. This result suggests us that NCNT itself can't be a desired support to promote the Ru NPs and the introduction of single-atom Ni changed the property of NCNT. The catalyst stability of Ru@Ni-NCNT/AC performed well, although the nanotube structure was damaged and transformed to nanosheet structure (Supplementary Fig 10 and 12).

**X-ray photoelectron spectra analysis of Ru on different supports**. It has been known that the bimetallic catalyst possesses higher catalytic activity of such as hydrogenation reaction and CWAO, induced by the synergetic interaction between different NPs and the support[6,13,14]. However, the Ni NPs on the surface of Ni-NCNT/AC has been removed by an acid-cleaning process, as proved by the result of Ni XAFS spectra and Ni 2p XPS spectra (Fig. 2 and Supplementary Fig. 5). The surface electron state of the Ru NPs just can be tuned by the support Ni-NCNT/AC. As support to Ru, Ni-NCNT/AC can stabilize the Ru NPs and tune the binding energy of Ru to 461.5 eV, while the binding energy of

**Fig. 2** Structural characterizations of single-Ni-atom catalyst by X-ray absorption spectroscopy. **a** Normalized Ni K-edge XANES spectra. **b** k3-weighted Fourier transform spectra from Ni K-edge EXAFS. **c** WT-EXAFS of Ni foil. **d** WT-EXAFS of NiO. **e** WT-EXAFS of Ni-NCNT/AC.
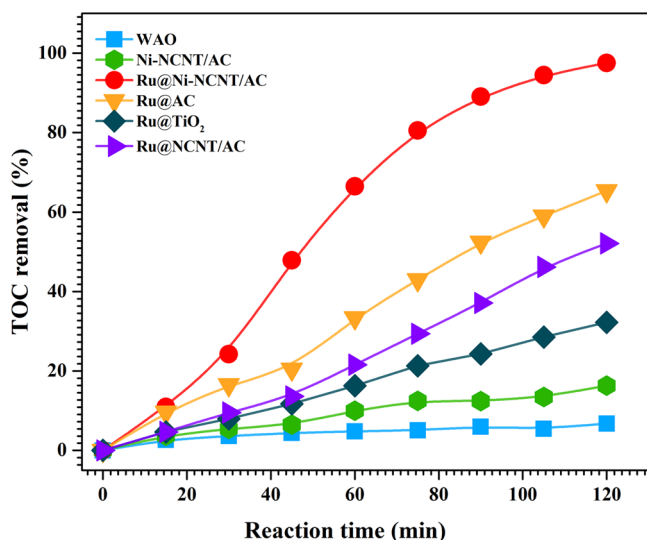


**Fig. 3** TOC removal performance in CWAO system using different catalysts.

$Ru^0$ in Ru@AC and Ru@TiO$_2$ are 462.1 eV and 463.8 eV. And we find the catalytic activity Ru on different support is corresponded with the binding energy of Ru (Fig. 4), which show that higher binding energy go against with the catalytic activity of Ru. Besides, we also noticed that there are RuO$_x$/Ru peaks appeared in Ru@Ni-NCNT/AC while Ru@AC and Ru@TiO$_2$ didn't appear (Fig. 4)[15]. The RuO$_x$/Ru peak in Ru@Ni-NCNT/AC is close to the Ru peak in Ru@TiO$_2$ which imply that some strong bonds between Ru and O atom formed. And this kind of oxidized Ru possess low catalytic activity towards acetic acid which can be inferred by the performance of Ru@TiO$_2$. And we deduced that

the RuO$_x$/Ru peak were mainly derived from Ru clusters supported on the AC base material of the Ni-NCNT/AC, since part of RuO$_x$/Ru peak is overlapped with the Ru$^0$ peak in Ru@AC. The Ru NPs on the AC base material of Ni-NCNT/AC is much smaller than that on AC support, while lots of Ru was supported on Ni-NCNT of Ni-NCNT/AC. The smaller Ru NPs are easier to form the stable Ru-O bond. Thus, the RuO$_x$/Ru peak was formed in the XPS of Ru@Ni-NCNT/AC. We also investigated the influence of Ru NPs size on AC support (Supplementary Fig. 11). The results show that larger Ru particles on the support are also not good to the catalysis process. Above all, we further confirmed the promoting effect of the support Ni-NCNT.

**Density-functional theory calculations**. Heterogeneous catalytic reactions begin with the adsorption of the reaction substrates. In CWAO system of acetic acid, there are two important sections affecting the reaction rate, the adsorption and activation of reactants. To activate these two reaction substrates, the adsorption step must occur on the surface of the heterogeneous catalyst firstly. Based on the density functional theory (DFT), we calculated the adsorption energy ($\Delta E_{ad}$) of O$_2$ and acetic acid on different catalyst model (Fig. 5 and Supplementary Table 3). And it's necessary to state the model here using Ru cluster is different from Ru NP we observed in TEM and may have some limitation on the following analysis, but the models still can represent some interaction between the support and active metal Ru. And the computational results show that the metal heteroatom Ni anchored into the nanotube will decrease the $\Delta E_{ad}$ towards the substrates, especially O$_2$ ($\Delta E_{ad-O2}$: from 1.23 eV to −0.06 eV), while the cluster on the CNT possess higher adsorption energy that adsorbs the substrates more easily (Fig. 5b, g, c, h and Supplementary Fig. 13a, b, g, h). That explained the low catalytic activity of Ni-NCNT/AC towards CWAO of acetic acid compared with Ru cluster outer of the nanotube. the CO-diffuse reflectance
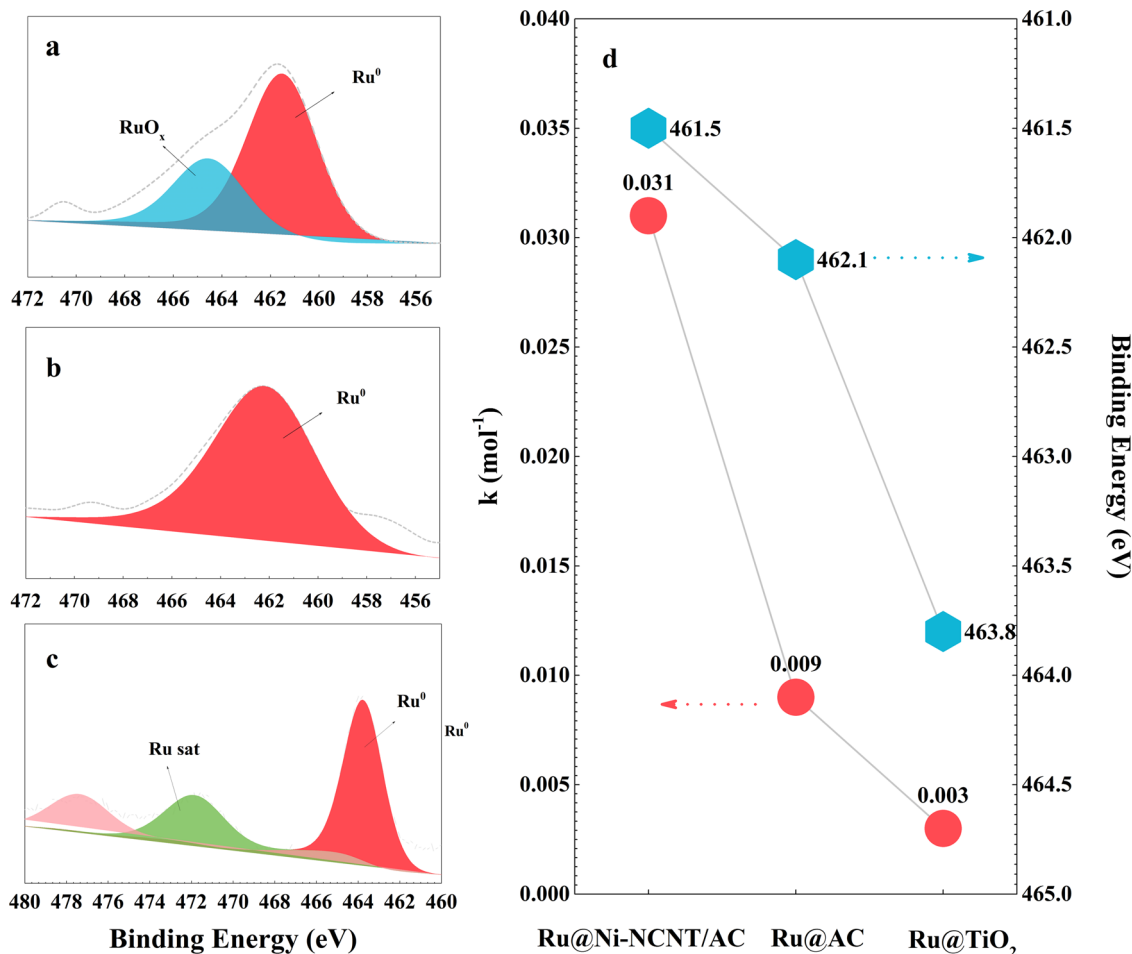
**Fig. 4** XPS Ru 3p spectra and performance of Ru particles on different supports (**a** Ru@Ni-NCNT/AC; **b** Ru@AC; **c** Ru@TiO$_2$; **d** the relationship between reaction rate constant k and binding energy of reduced Ru on different support).
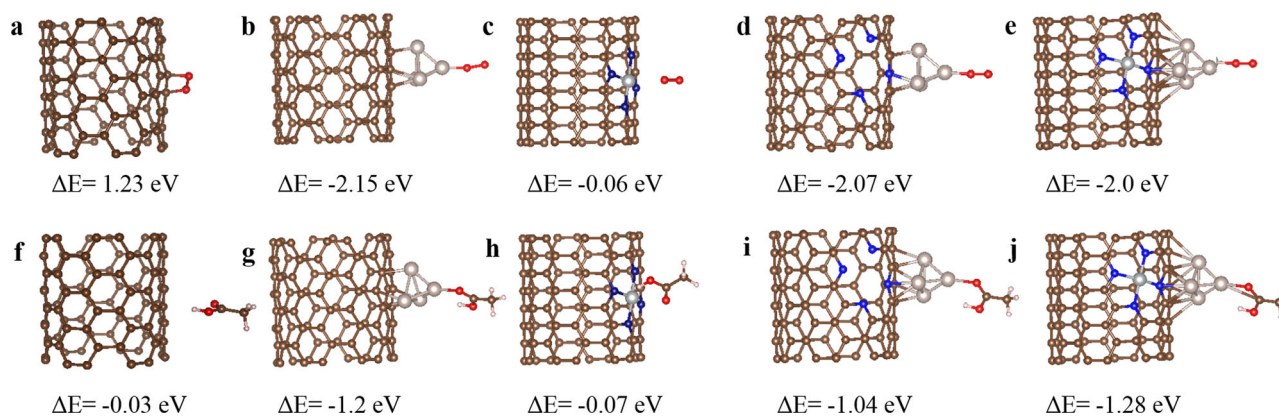


**Fig. 5** Adsorption configuration of O$_2$ and acetic acid on different support: **a** O$_2$ adsorbed on CNT; **b** O$_2$ adsorbed on Ru$_4$@CNT; **c** O$_2$ adsorbed on Ni-NCNT; **d** O$_2$ adsorbed on Ru$_4$@NCNT; **e** O$_2$ adsorbed on Ru$_4$@Ni-NCNT; **f** CH$_3$COOH adsorbed on CNT; **g** CH$_3$COOH adsorbed on Ru$_4$@CNT; **h** CH$_3$COOH adsorbed on Ni-NCNT; **i** CH$_3$COOH adsorbed on Ru$_4$@NCNT; **j** CH$_3$COOH adsorbed on Ru$_4$@Ni-NCNT.

infrared Fourier transform spectroscopy (CO-DRIFTS) also proved that anchored Ni in Ni-NCNT/AC has low adsorption ability (Supplementary Fig. 14). The noble metal Ru cluster intrinsically possess a high affinity for adsorbing and activating O$_2$ and acetic acid (Fig. 5b, g). Ru single-atom anchoring into the NCNT dramatically increased the $\Delta E_{ad}$ for O$_2$ and acetic acid which represents a charge redistribution (Supplementary Fig. 13a, b), while atom in Ru cluster will possess a better adsorption for O$_2$

and acetic acid (Fig. 5b, g). Thus, loading NPs on the support will be better for adsorbing O$_2$ and acetic acid. However, the strong bonded oxygen adsorbed on the NPs surface will poison the metal surface. Thus, the proper adsorption on the Ru cluster surface is vital important for catalytic oxidation reaction, especially at high-temperature and high-pressure condition. The Ru cluster on Ni-NCNT (−2.0 eV) show a very similar adsorption on O$_2$ than that of Ru cluster on NCNT (−2.07 eV), while the affinity for acetic

acid improved a lot for Ru cluster on Ni-NCNT compared with the Ru cluster on NCNT (Fig. 5d, e, i, j). From the computational result, it is confirmed that the modulation through doping single-atom Ni into NCNT makes the interaction between Ru cluster and support towards better adsorption state that is benefit for the catalytic reaction. Anchoring of metal atom can redistribute the charge of metal atom and the surrounding atoms and modified the property of base-materials[16]. The different adsorption configuration for acetic acid (Fig. 5g, i, j) has proved that single-atom Ni in Ni–NCNT redistribute the outer electron, affecting the surrounding atom to have a new electronic structure and further alters the material's electronegativity and promote the activity of Ru cluster[17].the reason of the adsorption for $O_2$ was less affected by introducing Ni single-atom may be that the new electronic structure was not suitable for $O_2$ to form Ru–O bond. Therefore, loading noble metal nanoparticle on this transition metal atom anchored support is a facile and reliable strategy for improving the catalytic activity.

## Discussion

In summary, we demonstrate the reasonable construction of a Ni single-atom confined NCNT superstructure serving as a support, with tunable interaction between the support and noble metal active site, for loading noble metal Ru for efficient CWAO of acetic acid, showing improved catalytic activity. The transition metal atoms anchored in the NCNT act as an "electron donor" to significantly tune the support electronegativity, and further modify the active sites on the surface through the super-conductive graphene sheet. This kind of catalyst possesses both high catalytic activity and stability, since the electron donor metal is anchored into the carbon skeleton, avoiding the metal leaching in bimetallic catalysis. We believe this work will provide a universal and reliable fabrication strategy of SACMs based supports for constructing high-performance catalysts with exceptional activity and stability in various energy conversion systems.

## Methods

**Catalysts preparation**. Ni-NCNT/AC: 6.0 g active carbon (AC, 200 mesh, a commercial coconut shell charcoal purchased from SuZhou TaiMei Activated Carbon CO.LTD) was immersed into 20 ml aqueous solution of $NiCl_2 \cdot 6H_2O$ ($Ni^{2+}$: 34.5 mg $ml^{-1}$) with stirring for 0.25 h under ultrasonic condition. The sample was put into a vacuum oven at 50 °C and −0.08 MPa for 6 h. the obtained powder was grinded with 10 g dicyandiamide (DCD) until there is no obvious white particle. The well-mixed powder was annealed at 400 °C under $N_2$ circumstance for 2 h to obtain reduced Ni nanoparticle and then further annealed at the 800 °C to obtain the NCNT superstructure. The pristine Ni-NCNT/AC conduct an acid-cleaning (1.0 mol $L^{-1}$ $H_2SO_4$, 5 h) process to remove the surface Ni on the nanotube. And then the sample were handled under a condition of 120 °C, 1.3 MPa ($N_2$) with 250 ml 1.0 mol $L^{-1}$ $H_2SO_4$ for 6 h. the obtained sample was washed till the eluate pH = 7. The sample were dried at 50 °C and −0.08 MPa for 6 h to obtain Ni-NCNT/AC.

Ru@ Ni-NCNT/AC: 3.0 g Ni-NCNT was immersed into 5 ml aqueous solution of $RuCl_3 \cdot H_2O$ ($Ru^{3+}$: 14.4 mg $ml^{-1}$) with stirring for 0.25 h under ultrasonic condition. And then the sample was put into a vacuum oven at 50 °C and −0.08 MPa for 6 h. The obtained powder was annealed at 800 °C under $N_2$ circumstance for 2 h to gain a reduced Ru (Supplementary Fig. 6) supported on the surface of the catalyst.

Ru@AC: 3 g AC was immersed into 10 ml aqueous solution of $RuCl_3 \cdot H_2O$ ($Ru^{3+}$: 7.2 mg $ml^{-1}$) with stirring for 0.5 h under ultrasonic condition. The sample was put into a vacuum oven at 50 °C and −0.08 MPa for 6 h. Then, the sample was annealed at 800 °C in a $N_2$ circumstance for 2 h. and then we get the Ru@AC catalyst without carbon nanotube superstructures.

Ru@TiO$_2$: 3 g TiO$_2$ powder (particle size is around 200 nm) was immersed into 10 ml aqueous solution of $RuCl_3 \cdot H_2O$ ($Ru^{3+}$: 7.2 mg $ml^{-1}$) with stirring for 0.5 h under ultrasonic condition. The sample was put into a vacuum oven at 50 °C and −0.08 MPa for 6 h. Then, the sample was annealed at 800 °C in a $N_2$ circumstance for 2 h. and then we get the Ru@TiO$_2$ catalyst.

Ru@NCNT: 1.0 g NCNT powder (tube diameter is 30–50 nm) was immersed into 10 ml aqueous solution of $RuCl_3 \cdot H_2O$ ($Ru^{3+}$: 2.4 mg $ml^{-1}$) with stirring for 0.5 h under ultrasonic condition. The sample was put into a vacuum oven at 50 °C and −0.08 MPa for 6 h. Then, the sample was annealed at 800 °C in a $N_2$ circumstance for 2 h. and then we got the Ru@NCNT catalyst.

Ru@NCNT/AC: 0.2 g NCNT powder (tube diameter is 30–50 nm) and 6.0 g AC were mixed through ball-milling method to obtain a composite support NCNT/AC. Then, 3 g NCNT/AC was immersed into 10 ml aqueous solution of $RuCl3 \cdot H_2O$ ($Ru^{3+}$: 7.2 mg $ml^{-1}$) with stirring for 0.5 h under ultrasonic condition. The sample was put into a vacuum oven at 50 °C and −0.08 MPa for 6 h. Then, the sample was annealed at 800 °C in a $N_2$ circumstance for 2 h. and then we get the Ru@NCNT/AC catalyst.

**Experiment evaluation**. The batch reactions were performed in a 500 mL batch reactor equipped with a magnetically driven stirrer and an electric heating jacket. The reactor was CJF-0.5 type autoclaves made of titanium alloy supplied by Dalian Tongda Autoclave Plant. In the standard procedure for a CWAO experiment, the catalyst (3.3 g $L^{-1}$, 200 ml) and acetic acid solution (4000 mg $L^{-1}$, 200 mL) were put into the autoclave. The autoclave was closed, filled with a 1.0 MPa pressure of nitrogen, then the heating-up program started. When the set temperature (250 °C) was attained, the oxygen was filled in quickly until the pressure reaching 6.0 MPa. The stirrer started at a speed of 400 rpm. This time was taken as the zero time of reaction and the reaction time was set as 120 min. The liquid samples were taken every 15 min from the sampling valve and filtered to remove any catalyst particle and finally analyzed. The total organic carbon (TOC) of samples were determined on a total organic carbon (TOC) analyzer (TOC-VCPH/CPN, Shimadzu, Japan) and the mineralization rate were calculated.

$$\text{The minalization rate} = \text{TOC removal} = \frac{C}{C_0} \times 100\% \qquad (1)$$

$C_0$: the total organic carbon of acetic acid solution at the beginning of the reaction when the temperature reaches 250 °C and oxygen was not filled in.

$C$: the total organic carbon of acetic acid solution when the reaction has proceeded for a certain time after the oxygen was filled in.

**Characterization**. Transmission electron microscopy (TEM) were carried out with FEI Tecnai G2 F20 transmission electron microscope operating at an accelerating voltage of 200 kV.High-resolution TEM (HRTEM), high-angle annular dark filed (HAADF) scanning transmission electron microscopy (STEM) studies, and energy dispersive X-ray (EDX) microanalysis were carried out with a JEM-ARM200F atomic resolution analytical microscope operating at an accelerating voltage of 200 kV. X-ray photoelectron spectra (XPS) was measured on a Thermo ESCALAB 250Xi spectrometer equipped with an Al anode (Al $K\alpha$ = 1846.6 eV), operated at 15 kV and 10.8 mA. Energy calibration was carried out using the C1s peak of adventitious C at 284.6 eV.

The specific surface area of SW catalysts was measured by the Brunauer–Emmett–Teller (BET) methods and was determined with N2 adsorption/desorption isotherms at 77 K using QUADRASORB SI4 instrument produced by Quantachrome Company. The catalyst samples prior to the adsorption measurement were degassed at 300 °C for 3 h under vacuum.

XAFS spectra at the Ni K-edge were measured at the beamline 1W1B station of the Beijing Synchrotron Radiation Facility (BSRF, 2.5 GeV, 250 mA, monochromatized with Si (111) double-crystals). The spectra of Ni-NCNT/AC samples were recorded in fluorescence mode using solid-state detector. The spectra of Ni foil and NiO references were recorded in transmission mode. The analysis of all EXAFS data was performed using Athena. For Ni K-edge spectra, spectra were background-subtracted using the following parameters: Rbkg = 1.0, and k-weight = 2. The Fourier transformation was conducted over k range of 3–12 Å-1. The wavelet transform analysis was also performed to confirm the surrounding of Ni.

CO-diffuse reflectance infrared Fourier transform spectroscopy (CO-DRIFTS) were undertaken on a Nicolet iS 50 Fourier-transform infrared spectrometer. The catalyst sample was heated to 300 °C in 5% H$_2$/Ar for 1 h to reduce the surface Ni species. And then the sample was cooled down to room temperature in such gas circumstance. Next, 1% CO/Ar was introduced into the system to for 1 h to adsorb the CO on the surface of the catalyst. then Ar was introduced to remove the residual CO and physically adsorbed CO and this moment was set as 0 min to collect the DRIFTS spectra and collect the other two spectra data in 3 min, 20 min. here, we choose Ni-NCNT/AC and the pristine Ni-NCNT/AC with Ni NPs on the surface of Ni-NCNT/AC(Ni NPs@Ni-NCNT/AC).

A total organic carbon (TOC) analyzer (TOC-VCPH/CPN, Shimadzu, Japan) was employed to determine the residual amounts of organic substances in the effluent.

Density functional theory calculations: all spin-polarized calculations are performed by using the first-principles plane-wave pseudopotential formulation[18–20] as implemented in the Vienna ab-initio Simulation Package (VASP). The exchange-correlation functional is in the form of Perdew-Burke-Ernzerhof (PBE)[21] with the generalized gradient approximation (GGA). The cutoff energy of 400 eV for the plane-wave basis, and Monkhorst-Pack k-mesh[22] of $1 \times 1 \times 4$ for the calculations are applied to insure the energy convergence is 1 meV and the residual force acting on each atom is <0.05 eV/Å. It should be noted that the Ru or Ni nanoparticle loaded C nanotubes are constructed by the $1 \times 1 \times 4$ supercell (6, 6) single-wall nanotube encapsulating a Ru$_4$ or Ni$_4$ cluster, which is widely used in the previous works[23,24]. To eliminate interactions between the nanotube and its periodic images, we use a vacuum distance larger than 12 Å for the rhombohedral supercell geometry.

## Data availability

## References

1. Wang, A., Li, J. & Zhang, T. Heterogeneous single-atom catalysis. *Nat. Rev. Chem.* **2**, 65–81 (2018).
2. Wang, Y. et al. Catalysis with two-dimensional materials confining single atoms: concept, design, and applications. *Chem. Rev.* **119**, 1806–1854 (2019).
3. Liu, J. Advanced electron microscopy of metal–support interactions in supported metal catalysts. *ChemCatChem* **3**, 934–948 (2011).
4. Chen, Y. et al. Single-atom catalysts: synthetic strategies and electrochemical applications. *Joule* **2**, 1242–1264 (2018).
5. Zhao, C. et al. Solid-diffusion synthesis of single-atom catalysts directly from bulk metal for efficient $CO_2$ reduction. *Joule* **3**, 584–594 (2018).
6. Fu, J. et al. Bimetallic Ru–Cu as a highly active, selective and stable catalyst for catalytic wet oxidation of aqueous ammonia to nitrogen. *Appl. Catal. B* **184**, 216–222 (2016).
7. Gallezot, P., Chaumet, S., Perrard, A. & Isnard, P. Catalytic wet air oxidation of acetic acid on carbon-supported ruthenium catalysts. *J. Catal.* **168**, 104–109 (1997).
8. Kim, K. H. & Ihm, S. K. Heterogeneous catalytic wet air oxidation of refractory organic pollutants in industrial wastewaters: a review. *J. Hazard. Mater.* **186**, 16–34 (2011).
9. Guo, S. et al. Probing the electronic effect of carbon nanotubes in catalysis: NH3 synthesis with Ru nanoparticles. *Chem. Eur. J.* **16**, 5379–5384 (2010).
10. Pintar, A., Batista, J. & Tišler, T. Catalytic wet-air oxidation of aqueous solutions of formic acid, acetic acid and phenol in a continuous-flow trickle-bed reactor over $Ru/TiO_2$ catalysts. *Appl. Catal. B* **84**, 30–41 (2008).
11. Liu, W. et al. Single-atom dispersed Co–N–C catalyst: structure identification and performance for hydrogenative coupling of nitroarenes. *Chem. Sci.* **7**, 5758–5764 (2016).
12. Cheng, Y. et al. Atomically dispersed transition metals on carbon nanotubes with ultrahigh loading for selective electrochemical carbon dioxide reduction. *Adv. Mater.* **30**, 1706287 (2018).
13. Zhu, L. et al. Effect of ruthenium nickel bimetallic composition on the catalytic performance for benzene hydrogenation to cyclohexane. *Appl. Catal. A* **499**, 124–132 (2015).
14. Zhu, L. et al. Ultrafine nanoparticle-supported Ru nanoclusters with ultrahigh catalytic activity. *Small* **11**, 4385–4393 (2015).
15. Morgan, D. J. Resolving ruthenium: XPS studies of common ruthenium materials. *Surf. Interface Anal.* **47**, 1072–1079 (2015).
16. Meyer, J. C. et al. Experimental analysis of charge redistribution due to chemical bonding by high-resolution transmission electron microscopy. *Nat. Mater.* **10**, 209 (2011).
17. Sun, J. et al. Freezing copper as a noble metal–like catalyst for preliminary hydrogenation. *Sci. Adv.* **4**, eaau3275 (2018).
18. Kresse, G. Ab initio molecular dynamics for liquid metals. *J. Non-Cryst. Solids* **192–193**, 222–229 (1995).
19. Kresse, G. & Hafner, J. Ab initio molecular-dynamics simulation of the liquid-metal–amorphous-semiconductor transition in germanium. *Phys. Rev. B* **49**, 14251–14269 (1994).
20. Kresse, G. & Furthmüller, J. Efficiency of ab-initio total energy calculations for metals and semiconductors using a plane-wave basis set. *Comput. Mater. Sci.* **6**, 15–50 (1996).
21. Perdew, J. P., Burke, K. & Ernzerhof, M. Generalized gradient approximation made simple [Phys. Rev. Lett. 77, 3865 (1996)]. *Phys. Rev. Lett.* **78**, 1396–1396 (1997).
22. Chadi, D. J. Special points for Brillouin-zone integrations. *Phys. Rev. B Condens. Matter* **16**, 5188–5192 (1977).
23. Deng, D. et al. Iron encapsulated within pod-like carbon nanotubes for oxygen reduction reaction. *Angew. Chem. Int. Ed.* **52**, 371–375 (2013).
24. Liu, C. et al. Improved field emission properties of double-walled carbon nanotubes decorated with Ru nanoparticles. *Carbon* **47**, 1158–1164 (2009).

## Acknowledgements

## Author contributions

C.S. and H.Z. supervised the progress of entire project. C.J. initiated the project and conceived the experiments, L.M. performed the XAFS and DFT calculation and contribute equally with C.J.; W.S., X.T, H.J., and Z.W. gave important suggestions on experiment designing and paper writing. C.J. and P.H. conducted the evaluation of catalysts. H.W. and M.L. performed the TEM, XPS, and CO-DRIFTS.

## Competing interests

The authors declare no competing interests.

## Additional information